

# Predicting trends in atmospheric CO<sub>2</sub> across the Mid-Pleistocene Transition using existing climate archives

Jordan R.W. Martin<sup>1</sup>, Joel Pedro<sup>2,3</sup>, Tessa R. Vance<sup>3</sup>

<sup>1</sup>Institute for Marine and Antarctic Studies, University of Tasmania, Hobart, 7004, Australia

<sup>2</sup>Australian Antarctic Division, Kingston, 7050, Australia

<sup>3</sup>Australian Antarctic Program Partnership, Institute for Marine and Antarctic Studies, University of Tasmania, Hobart, 7004, Australia

*Correspondence to:* Jordan R.W. Martin (jrmartin@utas.edu.au)

## Abstract

During the Mid-Pleistocene Transition (MPT), ca. 1200–800 thousand years ago (kya), the Earth's glacial cycles changed from 41 kyr to 100 kyr periodicity. The emergence of this longer ice-age periodicity was accompanied by higher global ice volume in glacial periods and lower global ice volume in interglacial periods. Since there is no known change in external orbital forcing across the MPT, it is generally agreed that the cause of this transition is internal to the earth system. Resolving the climate, carbon cycle and cryosphere processes responsible for the MPT remains a major challenge in earth and palaeoclimate science. To address this challenge, the international ice core community has prioritised recovery of an ice core record spanning the MPT interval.

Here we present results from a simple generalised least squares (GLS) model that predicts atmospheric CO<sub>2</sub> out to 1.5 Myr. Our prediction utilises existing records of atmospheric carbon dioxide (CO<sub>2</sub>) from Antarctic ice cores spanning the past 800 kyr along with the existing LR04 benthic  $\delta^{18}\text{O}_{\text{calcite}}$  stack (Lisiecki & Raymo, 2005; hereafter 'benthic  $\delta^{18}\text{O}$  stack') from marine sediment cores. Our predictions assume that the relationship between CO<sub>2</sub> and benthic  $\delta^{18}\text{O}$  over the past 800 thousand years can be extended over the last one and a half million years. The implicit null hypothesis is that there has been no fundamental change in feedbacks between atmospheric CO<sub>2</sub> and the climate parameters represented by benthic  $\delta^{18}\text{O}$ , global ice volume and ocean temperature.

We test the GLS-model predicted CO<sub>2</sub> concentrations against observed blue ice CO<sub>2</sub> concentrations,  $\delta^{11}\text{B}$ -based CO<sub>2</sub> reconstructions from marine sediment cores and  $\delta^{13}\text{C}$  of leaf-wax based CO<sub>2</sub> reconstructions (Higgins *et al.*, Yan *et al.*, 2019 and Yamamoto *et al.*, 2022). We show that there is not clear evidence from the existing blue ice or proxy CO<sub>2</sub> data to reject our predictions nor our associated null-hypothesis. A definitive test and/or rejection of the null hypothesis may be provided following recovery and analysis of continuous oldest ice core records from Antarctica, which are still several years away. The record presented here should provide a useful comparison for the oldest ice core records and opportunity to provide further constraints on the processes involved in the MPT.

39

## 40 **1 Introduction**

41 Ice core records from Antarctica provide comprehensive and continuous records of many climate parameters  
42 over the last 800 thousand years, e.g. from the Vostok (Petit *et al.*, 1999) and European Project for Ice Coring in  
43 Antarctica's Dome-C (EDC) ice cores (Jouzel *et al.*, 2007). One of the major challenges in climate science lies  
44 beyond the current threshold of the ice core record. The Mid-Pleistocene Transition (MPT) spans from ca.  
45 1200–800 thousand years ago (kya) (Chalk *et al.*, 2017) and is characterised by a change from regularly paced  
46 40 thousand year (kyr) glacial cycles with thinner glacial ice sheets to quasi-periodic 100 kyr glacial cycles in  
47 which ice sheets are more persistent and thicker (Clark *et al.*, 2006, Chalk *et al.*, 2017). To resolve the forcings  
48 and feedbacks involved in this transition, multiple nations are targeting recovery of continuous ice cores  
49 spanning the MPT under the framework of the International Partnerships in Ice Core Science (IPICS) oldest ice  
50 core challenge (IPICS, 2020).

51

52 The purpose of the current study is to make a simple prediction of atmospheric CO<sub>2</sub> across the MPT. Cross-  
53 comparison of our and other predicted CO<sub>2</sub> records against observed MPT CO<sub>2</sub> data will aid in testing  
54 competing hypotheses on the cause of the transition, in particular the role of carbon cycle changes.

55

56 The MPT occurred in the absence of any changes to orbital insolation forcing, therefore, the mechanisms behind  
57 the MPT must be internal to the earth system (Raymo, 1997; Ruddiman *et al.*, 1989). Multiple hypotheses have  
58 been put forward to explain the transition. A common element in many of these, is internal climate/earth system  
59 changes which allow for the development of thicker, more extensive ice sheets that could endure insolation  
60 peaks corresponding to the 23 kyr precession and 41 kyr obliquity cycles, i.e., an increase in the threshold for  
61 deglaciation and altered sensitivity to orbital forcings (McClymont *et al.*, 2013; Tzedakis *et al.*, 2017). Indeed,  
62 the skipped obliquity cycle hypothesis, proposes that 100 kyr signal seen in spectral analysis of the post-MPT  
63 benthic  $\delta^{18}\text{O}$  stack (e.g. Fig 1A) may be comprised of alternating 80 and 120-kyr signals, i.e. in which the  
64 intervening obliquity cycles are skipped. Among the prominent hypotheses to explain an increased threshold for  
65 deglaciation are the following three.

66 1) A long- term decrease in radiative forcing due to a secular reduction in atmospheric CO<sub>2</sub> across the  
67 transition (e.g. Berger *et al.*, Hönisch *et al.*, 2009; 1999, Raymo *et al.*, 1988). According to this view,  
68 reduced radiative forcing drives the formation of larger and more stable ice sheets.

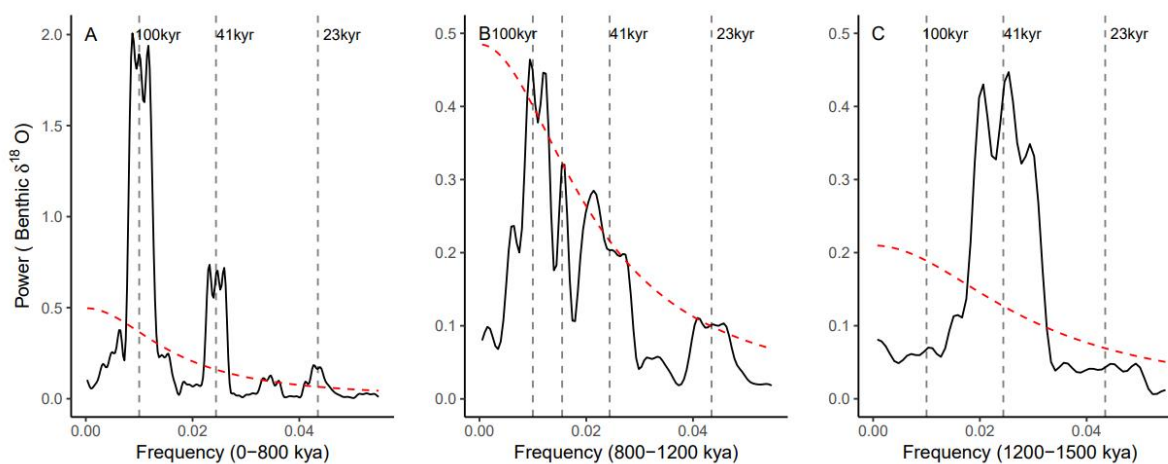
69 2) Progressive removal of sub-glacial regolith during the 41 kyr glacial cycles. Clark & Pollard (1998)  
70 proposed that ice sheet basal sliding prior to the MPT was enhanced by the presence of a low-friction  
71 sedimentary regolith layer between the Laurentide ice sheet and the crystalline bedrock. According to  
72 this view, progressive removal of this sedimentary layer then favoured the development of larger and  
73 more persistent post-MPT ice sheets.

74 3) Phase-locking of the Northern and Southern Hemisphere ice sheets. In frequency spectra of the global  
75 marine benthic  $\delta^{18}\text{O}$  record (Fig. 1) there is no evidence of the precession (23 kyr) component of  
76 northern hemisphere insolation prior to the MPT; the spectra is dominated by the obliquity (41 kyr)  
77 component (Fig. 1C). Emergence of significant precession and 100 kyr signals occurs across the MPT  
78 (Fig. 1B), and all three components are clearly present after the MPT (Fig. 1A). Raymo *et al.* (2006)

79 suggested that precession-paced changes in northern and southern hemisphere ice volumes may have  
 80 occurred prior to the MPT, but are cancelled due to out-of-phase ice volume changes between the two  
 81 hemispheres (Raymo & Huybers, 2008). According to this view, during the MPT the precession-paced  
 82 changes to fall into phase between the two hemispheres, such that the precession signal emerges  
 83 (Raymo *et al.*, 2006). In this view the global synchronisation of ice volume drives the formation of  
 84 larger and more stable ice sheets.

85  
 86 These hypotheses are not mutually exclusive. For a recent review on the cause of the MPT see Berends *et al.*  
 87 (2021a).

88



89

90

91 **Figure 1: Thomson Multi-taper Method (MTM) spectral analysis representing relative power of signal periodicity for:**  
 92 **A) Benthic  $\delta^{18}O$  stack after (0–800 kya) the Mid-Pleistocene Transition (MPT); B) Benthic  $\delta^{18}O$  across the MPT (800–**  
 93 **1200 kya); C) Benthic  $\delta^{18}O$  prior to the onset of the MPT (1200 kya–1500 kya). Each with a robust AR (1) 95 %**  
 94 **Confidence interval (red dashed line). Benthic  $\delta^{18}O$  stack data from Lisiecki and Raymo (2005).**

95

96 For a long-term decrease in radiative forcing by atmospheric  $CO_2$  to be the cause of the MPT, the reduction in  
 97  $CO_2$  would be expected in both glacial and interglacial stages (Chalk *et al.*, 2017). However, low resolution  
 98 boron-isotope-based  $CO_2$  reconstructions by Hönisch *et al.*, (2009), and Chalk *et al.*, (2017) suggest that glacial-  
 99 stage  $CO_2$  drawdown occurred over the MPT in the absence of interglacial  $CO_2$  drawdown. Glacial-stage  $CO_2$   
 100 draw-down across the MPT may be a positive climate-carbon cycle feedback to changes in ice sheet dynamics,  
 101 including  $CO_2$  drawdown by enhanced iron fertilisation of the Southern Ocean in response to exposed  
 102 continental shelves due to lower sea level, as well as planetary drying associated with colder climate conditions  
 103 (Chalk *et al.*, 2017). Colder glacial temperatures that enhance the solubility of  $CO_2$  in the oceans, and reduced  
 104 abyssal ocean ventilation has also been implicated in enhanced glacial-stage ocean storage of  $CO_2$  (McClymont  
 105 *et al.*, 2013; Hasenfratz *et al.*, 2019).

106

107 Testing of hypotheses on the cause of the MPT is currently limited by the lack of a continuous ice core that  
 108 spans its duration. The International Partnership in Ice Core Sciences (IPICS) has nominated recovery of such a  
 109 record as a key priority in ice core research (IPICS, 2020). Multiple national and international projects have

110 commenced, or are soon to commence, drilling for ‘oldest ice’ (see e.g. Shugi, 2022). In this project, we take  
111 inspiration from the “EPICA Challenge” in which the paleoclimate and modeling community was challenged to  
112 predict the global atmospheric carbon dioxide and methane concentrations from 800–400 kya based on the  
113 existing 400 kyr Vostok ice core record (Wolff *et al.*, 2004). Here, we use a generalised least squares (GLS)  
114 model trained on continuous climate archives to predict a CO<sub>2</sub> record out 1.5 Mya. We utilise two primary data  
115 sets for the GLS model: the existing 800 kyr ice core composite record of atmospheric CO<sub>2</sub> (Bereiter *et al.*,  
116 2015) and the LR04 benthic stack of 52 globally-distributed records of the <sup>18</sup>O to <sup>16</sup>O ratio of fossil benthic  
117 foraminifera calcite (hereafter referred to as the LR04  $\delta^{18}\text{O}$  benthic stack). The  $\delta^{18}\text{O}$  ratios in the LR04 benthic  
118 stack are governed primarily by deep ocean temperature and global ice volume at the time the foraminifera  
119 lived, with higher values indicating both increased ice volume and a colder climate. The relationship between  
120 the ice volume and ocean temperature components contributing to the  $\delta^{18}\text{O}$  benthic stack are not linear.  
121 Separating the two signals remains challenging and has been attempted elsewhere using a range of approaches  
122 from comparison with paired deep ocean temperature proxies (Elderfield *et al.*, 2012), inverse modelling  
123 (Berends *et al.*, 2021b) and spectral analysis (e.g. Huybers and Wunsch, 2009).

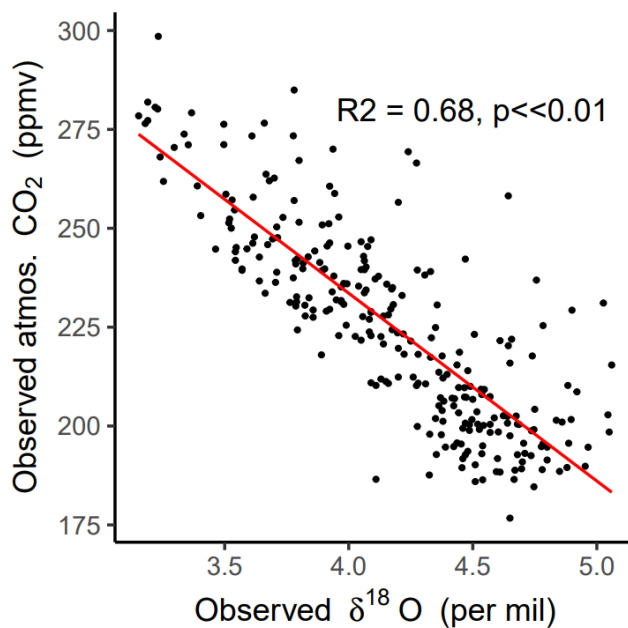
124  
125 Fig. 2 shows a scatter-plot of the LR04  $\delta^{18}\text{O}$  benthic stack versus observed ice core CO<sub>2</sub> over the past 800 kyr.  
126 Both data sets are binned to equivalent 3-kyr time steps (Methods). The Pearson’s correlation coefficient ( $r$ )  
127 between the data sets is -0.82 ( $p < 0.05$ ) indicating that ~68% of the variance in observed CO<sub>2</sub> is shared with the  
128 LR04  $\delta^{18}\text{O}$  benthic stack. This strong relationship provides an initial rationale for using the LR04  $\delta^{18}\text{O}$  benthic  
129 stack as an input parameter to predict CO<sub>2</sub> beyond 800 kyr. Mechanistically, multiple processes are expected to  
130 contribute to the shared variance. A first order factor is the dependency of CO<sub>2</sub> solubility on ocean temperature  
131 (e.g. Millero, 1995). From the simple solubility perspective, colder climate states with increased ice volume and  
132 colder ocean temperatures will drive increased ocean uptake of CO<sub>2</sub> (Berends *et al.*, 2021a). However, the  
133 solubility effect only accounts for a portion of observed glacial CO<sub>2</sub> drawdown (Archer *et al.*, 2000). Multiple  
134 additional contributors to the shared variance are proposed in the literature. These include (not exhaustively),  
135 direct radiative forcing of ice volume changes by CO<sub>2</sub> (e.g. Shackleton *et al.*, 1985); the impact of ice  
136 volume/sea level changes on atmospheric CO<sub>2</sub> via ocean productivity and carbonate chemistry changes (e.g.  
137 Broecker, 1982; Archer *et al.*, 2000; Ushie and Matsumoto, 2012); CO<sub>2</sub> drawdown during periods of high ice  
138 volume by increased iron fertilisation (e.g. Röthlisberger *et al.*, 2004; Martinez-Garcia *et al.*, 2014) and  
139 enhanced sea ice extent during periods of high ice volume capping the ventilation of CO<sub>2</sub> from the ocean  
140 interior at high latitudes (Stephens and Keeling, 2000).

141  
142 A quantitative separation and attribution of the processes linking global ice volume, ocean temperature and  
143 atmospheric CO<sub>2</sub> on millennial to orbital timescales is not currently available (e.g. Archer *et al.*, 2000; Sigman  
144 *et al.*, 2010; Gottschalk *et al.*, 2019) and will not be attempted here. Rather, we make the simple assumption that  
145 the relationships between the LR04 benthic  $\delta^{18}\text{O}$  stack and CO<sub>2</sub> can be extended beyond 800 kya and use  
146 generalised least squares (GLS) regression modelling between benthic  $\delta^{18}\text{O}$  and CO<sub>2</sub> to make a prediction of  
147 CO<sub>2</sub> spanning 800–1500 kya. The deliberately simple implicit assumption, and null hypothesis, is that there is  
148 no change to the feedback processes linking benthic  $\delta^{18}\text{O}$  and CO<sub>2</sub> before and after the MPT.

149

150 This approach differs to previous more complex model studies that have attempted to reconstruct CO<sub>2</sub> using the  
151 LR04 benthic δ<sup>18</sup>O stack as an input variable (van de Wal, 2011; Stap *et al.*, 2016, Berends *et al.*, 2021b). The  
152 latter studies use an inverse forward modelling approach, in which climate and ice sheet models of various  
153 complexities are used to capture physical relations between CO<sub>2</sub>, global temperature and ice volume. For  
154 example, in Berends *et al.*, 2021b the offset between modelled and observed benthic δ<sup>18</sup>O is used to calculate a  
155 value for atmospheric CO<sub>2</sub> that is iterated back to the inverse model. The CO<sub>2</sub> record which minimises the  
156 difference between the modelled and observed benthic stack is then taken as an estimate of how atmospheric  
157 CO<sub>2</sub> may have evolved to force coupled climate, deep ocean temperature and land ice volume changes that  
158 reproduce the observed benthic δ<sup>18</sup>O signal. Accuracy of the reconstructions in the inverse modelling approach  
159 depends on the ability of the climate and ice sheet models used to capture the correct climate dynamics across  
160 the MPT. Our GLS method is a simpler statistical approach, designed with the specific null hypothesis in mind,  
161 that does not attempt to simulate the physics linking benthic δ<sup>18</sup>O signal, land ice volume, global temperature  
162 and CO<sub>2</sub>. A range of approaches to reconstructing CO<sub>2</sub> have been called for and are of value in the context of  
163 forthcoming continuous ice core records across the MPT from oldest ice projects currently underway in  
164 Antarctica [IPICS 2020].

165  
166  
167



168 **Figure 2: Scatter plot of the composite observed atmospheric CO<sub>2</sub> record (Bereiter *et al.*, 2015) against**  
169 **the LR04 benthic stack of marine δ<sup>18</sup>O records (Lisiecki & Raymo, 2005). Red line is a linear line of best**  
170 **fit ( $R^2 = 0.68$ ;  $p < 0.05$ ).**

171  
172

173 To test our null hypothesis, in advance of the recovery of a continuous ice core, we compare our predicted CO<sub>2</sub>  
174 record to two sets of low-resolution ice core data that exist outside the current 800 kyr observed CO<sub>2</sub>. These data  
175 come from direct CO<sub>2</sub> measurements from ancient “blue ice” from the Allan Hills in East Antarctica (hereafter

176 referred to as BI-CO<sub>2</sub>) from ca. 1 Mya (Higgins *et al.*, 2015) and 1.5 Mya (Yan *et al.*, 2022). We use the term  
177 blue ice to describe deep, ancient glacial ice that has been brought nearer to the surface of an ice sheet by ice  
178 flow. Blue ice is sampled by cutting trenches or shallow drilling of up to several hundred meters (e.g. Higgins *et*  
179 *al.*, 2015). The vertical migration of blue ice is associated with high deformation making the ice samples  
180 stratigraphically complex and hard to date (Higgins *et al.*, 2015). As a result, blue ice records alone do not  
181 provide a continuous CO<sub>2</sub> record across the MPT. In the Discussion, we also compare our predicted record to  
182 existing proxy-CO<sub>2</sub> reconstructions from boron-isotope analysis of benthic foraminifera in marine sediment  
183 records (Chalk, *et al.*, 2017; Dyez *et al.*, 2018; Guillermic *et al.*, 2022), leaf wax δ<sup>13</sup>C carbon isotope ratios  
184 (Yamamoto *et al.*, 2022) and predictions from previous models of various complexities (van de Wal *et al.*, 2011;  
185 Willeit *et al.* 2019; Berends *et al.* 2021b). We conclude with discussion of the implications of our results and  
186 data-comparisons for the understanding MPT dynamics.

187  
188

## 189 **2 Methods**

190

191 We use a generalised least squares (GLS) model with an auto-regressive (AR) factor 1 to predict atmospheric CO<sub>2</sub>  
192 from the LR04 benthic δ<sup>18</sup>O stack (Fig. 3A and B). We use GLS because the assumptions of ordinary least squares  
193 (OLS) are violated by the presence of autocorrelation and heteroskedasticity in the regression errors. We selected  
194 the AR(1) correlation factor as it yielded the lowest Akaike information criterion (AIC) value from a test of  
195 multiple correlation factors. The AR(1) process assumes and accounts for dependence of error at a given point in  
196 time on the previous error term. In practise this makes the model assumptions more realistic and improves  
197 parameter estimation where, as in the climate system, observations are dependent on past values.

198

199 To obtain common time steps and resolution between the predictor (LR04 benthic δ<sup>18</sup>O stack) and response  
200 (CO<sub>2</sub>) variables, we re-grid the LR04 benthic stack and Bereiter *et al.*, (2015) CO<sub>2</sub> data into time bins with a  
201 resolution of 3-kyr. The GLS regression model was then applied over the 0 – 800 kyr range of the predictor and  
202 response variables as follows:

203

$$204 \quad CO_2 = 33.37 \times \delta^{18}O + 365.15, \text{ autoregressive (AR) factor: } 1$$

205

206 Based on the regression model, the δ<sup>18</sup>O values of the LR04 Benthic Stack from 800 – 1500 kya were used to  
207 predict CO<sub>2</sub> concentration over this range (hereafter referred to as PRED-CO<sub>2</sub>). To gauge the GLS model  
208 stability we took a bootstrap approach, selecting a random 50% subset of our data (with replacement) and re-  
209 running the model 1000 times to determine 95% confidence intervals for the predictions. While the GLS method  
210 itself addresses autocorrelation, the bootstrap method introduces variability such that each iteration of the model  
211 has different combinations of the original data points (including repeated ones), this variability helps in  
212 assessing the robustness and sensitivity of the model e.g. to variable data and dating uncertainty.

213

214 Uncertainties in the independent age scales of both the LR04 stack and the compiled CO<sub>2</sub> record are inherited by  
215 our GLS model and its predictions. The LR04 stack includes 57 globally-distributed benthic δ<sup>18</sup>O sediment core  
216 records. The age models for these cores are independently constructed from the average sedimentation rates of

217 each core, assuming global sedimentation rates have remained relatively stable, and with tuning to a simple ice  
218 model based on 21 June insolation at 65°N (Lisiecki & Raymo, 2005). The authors estimate uncertainty of 6 kyr  
219 from 1.5 – 1.0 Mya and 4 kyr from 1 – 0 Mya (Lisiecki & Raymo, 2005). The observed CO<sub>2</sub> composite ice core  
220 record for the past 800 kya (Bereiter et al., 2015) uses six independent dating methods for various core locations  
221 both spatially across Antarctica, and stratigraphically for different sections of the same core. The age uncertainty  
222 in the gas timescale has a median over the 0 – 800 kya interval of 2 kyr, but individual uncertainties can reach  
223 up to 5 kyr (Veres *et al* 2013; Bazin *et al.*, 2013). The relative age uncertainties between these input variables  
224 may diminish the regression or in some instances lead to spurious correlation. However, we expect any such  
225 effects are minor on the basis that our predictions show little sensitivity (median, 2 $\sigma$ , 5.78 ppm) to the bootstrap  
226 analysis (see Fig. 3B, C and Discussion).

227

### 228 **3 Results**

229 Fig. 3B shows the time series of our LR04 benthic  $\delta^{18}\text{O}$  stack-based GLS model predictions of atmospheric CO<sub>2</sub>  
230 (PRED-CO<sub>2</sub>) over the past 800 kyr, in comparison to the observed ice core CO<sub>2</sub> record from Bereiter et al.,  
231 (2015). The correlation coefficient ( $R^2$ ) between the predicted and observed records is 0.68 ( $p \ll 0.01$ ). Our  
232 PRED-CO<sub>2</sub> record out to 1.5 Mya with shaded 95% CIs from the bootstrap analysis is also shown, overlain with  
233 observed Allan Hills blue ice CO<sub>2</sub> (BI-CO<sub>2</sub>) datasets of age  $1000 \pm 89$  kya (Higgins *et al.*, 2015) and  $1.5 \text{ Mya} \pm$   
234  $213$  kyr (Yan *et al.*, 2022).

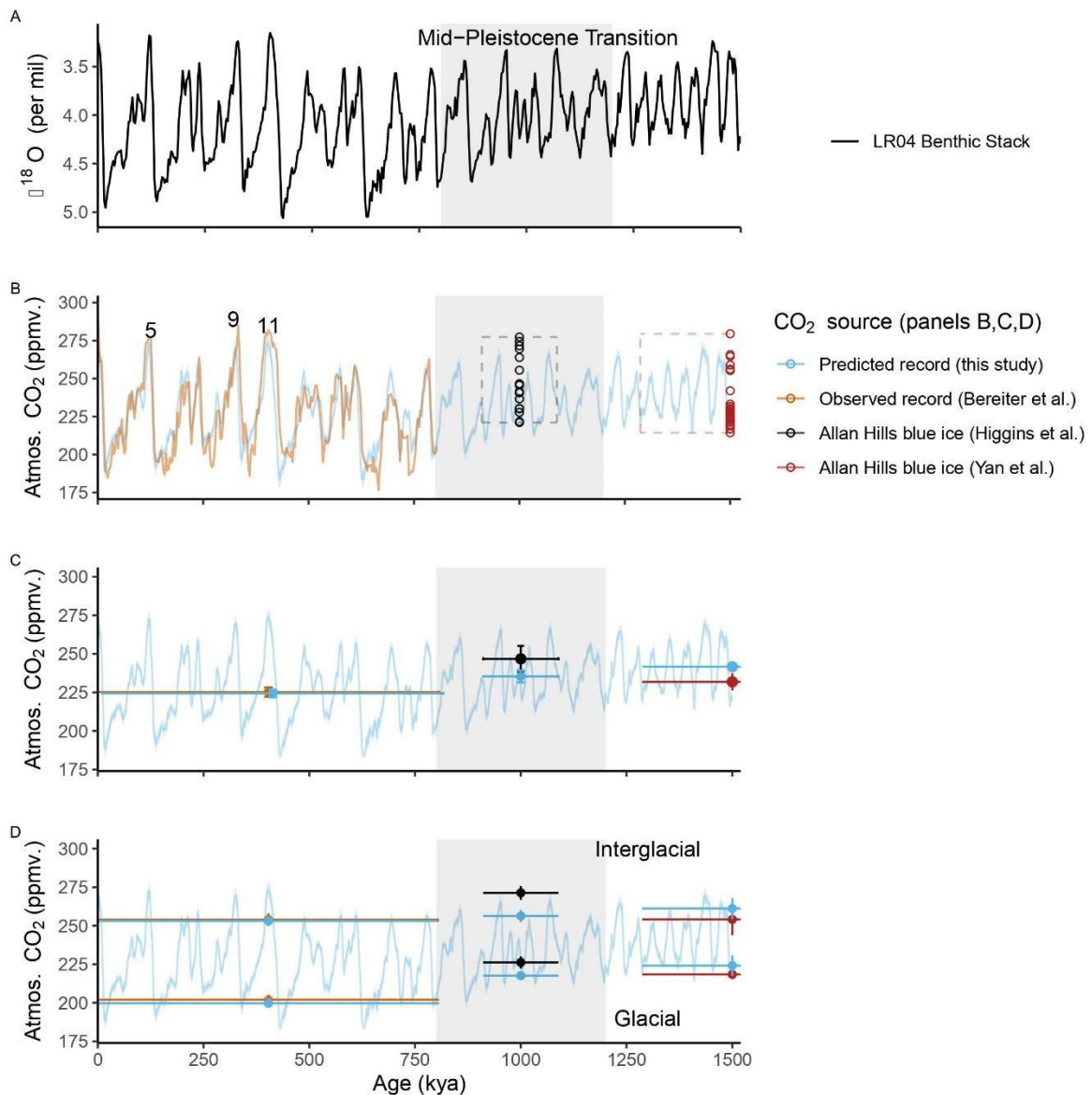
235

236 We evaluate the PRED-CO<sub>2</sub> record against the observed CO<sub>2</sub> data according to criteria of mean concentrations  
237 across the common intervals, and mean concentrations in the glacial and interglacial subsets of the data. First,  
238 the mean CO<sub>2</sub> concentration over the common intervals (Fig 3C). From 0–800 kya the mean concentration in  
239 observed (Bereiter et al., 2015) and PRED-CO<sub>2</sub> data are in close agreement ( $225.2 \pm 3.03$  ppm versus the  
240 predicted  $225.1 \pm 2.5$  ppm respectively; uncertainties are 95% confidence intervals, i.e.  $1.96\sigma$ ). In the  $1000 \pm 89$   
241 kya interval (i.e. averaged across the age uncertainty of the Higgins *et al.* (2015) blue ice data) the BI-CO<sub>2</sub>  
242 concentration is  $\sim 11$  ppm higher than PRED-CO<sub>2</sub> ( $246.7 \pm 8.4$  ppm versus the predicted  $235.5 \pm 3.9$  ppm), this  
243 difference is not significant at the 95% confidence level. For the  $1.5 \text{ Mya} \pm 213$  kyr interval, the mean BI-CO<sub>2</sub>  
244 concentration is  $\sim 10$  ppm lower than PRED-CO<sub>2</sub> ( $231.9 \pm 5.6$  ppm versus the predicted  $241.7 \pm 2.5$  ppm),  
245 which is marginally significant at the 95% level. Comparisons of mean levels across intervals spanning multiple  
246 glacial and interglacial cycles may be biased if (as is likely) the blue ice data is not sampling glacial and  
247 interglacial values with the same uniformity as a continuous record.

248

249 To address this, we define the glacial and interglacial thresholds of PRED-CO<sub>2</sub> to be respectively the lower and  
250 upper 25<sup>th</sup> percentiles of the LR04  $\delta^{18}\text{O}$  predictor variable (following Chalk *et al.*, 2017). Filtering the observed  
251 (Bereiter et al., 2015) CO<sub>2</sub> record and our predicted CO<sub>2</sub> record according to these definitions we find a very  
252 close match for glacial ( $202.0 \pm 3.2$  versus the predicted  $199.7 \pm 1.7$  ppm) and interglacial intervals ( $253.9 \pm 4.1$   
253 ppm versus the predicted  $253.1 \pm 2.3$  ppm), over the past 800 kya (see Fig. 3D). For blue ice (BI-CO<sub>2</sub>) data, a  
254 corresponding LR04 isotope signal could not be confidently applied to the measured CO<sub>2</sub> concentration due to  
255 the uncertainties associated with blue ice dating ; therefore, we defined the glacial and interglacial thresholds of  
256 blue ice data according to the top (interglacial) and bottom (glacial) 25<sup>th</sup> percentiles of actual CO<sub>2</sub>. Applying this

257 to the  $1000 \pm 89$  kya interval finds that observed BI-CO<sub>2</sub> data is  $\sim 9$  ppm higher than PRED-CO<sub>2</sub> during the  
 258 glacial stages ( $226.2 \pm 4.0$  ppm versus the predicted  $217.6 \pm 2.3$  ppm) and  $\sim 15$  ppm higher than PRED-CO<sub>2</sub>  
 259 during the interglacial stages ( $271.3 \pm 4.5$  versus the predicted  $256.3 \pm 3.8$  ppm). These differences are  
 260 significant with respect to the constrained uncertainties. In contrast, during the 1.5 Mya  $\pm 213$  kyr interval, the  
 261 mean BI- CO<sub>2</sub> concentration is not significantly different to PRED-CO<sub>2</sub> in either glacial ( $217.6 \pm 2.3$  versus the  
 262 predicted  $224.2 \pm 6.6$  ppm) or interglacial stages ( $256.3 \pm 3.8$  versus the predicted  $261.1 \pm 6.3$  ppm). These  
 263 comparisons, particularly the agreement at 1.5 Myr, indicate that PRED-CO<sub>2</sub> is not drifting systematically away  
 264 from the existing observed BI-CO<sub>2</sub> data. In our view the disagreement at 1.0 Myr, where BI-CO<sub>2</sub> is elevated  
 265 with respect to PRED-CO<sub>2</sub>, does not give sufficient cause to reject the GLS model, it could of course be a  
 266 failing in the model and/or could be due to potential biases in the blue ice data, for example elevated CO<sub>2</sub>  
 267 concentrations due to in-situ CO<sub>2</sub> production in blue ice (see Discussion).  
 268



269 **Figure 3: A) The LR04 Benthic Stack of 57 globally distributed  $\delta^{18}\text{O}$  records (Lisiecki & Raymo, 2005).**  
 270 **B) Comparison of our PRED-CO<sub>2</sub> (ppm) record to the current continuous composite record (0–800 kya);**  
 271



272 and to direct CO<sub>2</sub> measurements from Allan Hills blue ice cores (BI-CO<sub>2</sub>) ca. 1 Mya ( $\pm$  89 kyr) (Higgins *et*  
273 *al.*, 2015) and ca. 1.5 Mya ( $\pm$  213 kyr) (Yan *et al.*, 2022). Age uncertainty boundaries for the BI-CO<sub>2</sub> data  
274 are represented by dashed box boundaries. Marine isotope stages 5, 9, and 11 are numbered on the plot  
275 according to Lisiecki & Raymo (2005). Blue shading around PRED-CO<sub>2</sub> is the 95% CI from bootstrap  
276 analysis. C) Mean concentrations of the PRED-CO<sub>2</sub> and observed composite CO<sub>2</sub> records over the range  
277 of the observed composite record (offset for clarity), and the mean concentrations of the PRED-CO<sub>2</sub> and  
278 BI-CO<sub>2</sub> data at 1 Mya and again at 1.5 Mya averaged over the age uncertainty range of each BI-CO<sub>2</sub> data  
279 set. D) As for C) however filtered by the upper and lower 25<sup>th</sup> and 75<sup>th</sup> percentiles to estimate glacial and  
280 interglacial periods.

281

282 We now consider long-term trends in interglacial and (separately) glacial CO<sub>2</sub> levels across the past 1.5 Myr in  
283 PRED-CO<sub>2</sub> and in the existing ice core CO<sub>2</sub> data. For PRED-CO<sub>2</sub> there is no significant difference between CO<sub>2</sub>  
284 concentrations in the interglacial stages of the 1.5 Mya  $\pm$  213 kya, 1000  $\pm$  89 kya and 0–800 kya windows (Fig 4  
285 D, blue bars). In the ice core observations, interglacial levels at 1.5 Mya in BI-CO<sub>2</sub> are also within the  
286 uncertainties of those in the 0–800 kya interval. Notably, the BI-CO<sub>2</sub> concentrations in the 1000  $\pm$  89 kya  
287 interval appear elevated with respect to the 0–800 kyr and 1.5 Mya  $\pm$  213 kya intervals, however this elevated  
288 (ca. 271 ppm) level is consistent with the observed interglacial CO<sub>2</sub> concentration during interglacials 5, 9 and  
289 11 (Fig 3B). Overall, there is no indication in the observed ice core CO<sub>2</sub> data or in PRED-CO<sub>2</sub> for a long-term  
290 trend in *interglacial* CO<sub>2</sub> levels across the past 1.5 Myr.

291

292 In comparison, there are significant declines in glacial CO<sub>2</sub> levels across the MPT in PRED-CO<sub>2</sub> and the  
293 observed ice core data. For PRED-CO<sub>2</sub>, glacial CO<sub>2</sub> concentrations are not significantly different during the 1.5  
294 Mya  $\pm$  213 kya and 1000  $\pm$  89 kya windows. However, across the MPT, PRED-CO<sub>2</sub> glacial concentrations drop  
295 by  $\sim$ 18 ppm. This pattern is consistent with the observed data, where glacial CO<sub>2</sub> levels are also not significantly  
296 different between the 1.5 Mya  $\pm$  213 kya and 1000  $\pm$  89 kya windows ( $217.6 \pm 2.3$  and  $226.2 \pm 4.0$  ppm,  
297 respectively) and then fall by 24 ppm to the 0–800 kyr observed glacial mean of  $202.0 \pm 3.2$  ppm. Glacial-stage  
298 draw-down of CO<sub>2</sub> across the MPT in the absence of interglacial draw-down is consistent with previous  
299 observations based on the boron-isotope-based CO<sub>2</sub> reconstructions (e.g., Chalk *et al.*, 2017; Hönisch *et al.*,  
300 2009 and see Discussion). In the following section we also compare PRED-CO<sub>2</sub> data to boron-isotope-based and  
301 other CO<sub>2</sub> proxy records covering the 0 to 1.5 Myr interval.

302

#### 303 **4 Discussion**

304 Our objective with this manuscript was to generate the simplest reasonable model to predict CO<sub>2</sub> from the LR04  
305  $\delta^{18}\text{O}$  benthic stack and to test the predictions against available observations. It is possible that the fit between  
306 observed and our predicted CO<sub>2</sub> data could be further improved using a non-linear approach. However, we  
307 refrain from a non-linear approach for several key reasons. First, a scatter plot of the LR04  $\delta^{18}\text{O}$  benthic stack  
308 versus observed ice core CO<sub>2</sub> over the past 800 kyr yields a Pearson's correlation coefficient (R) of -0.82 (Fig.  
309 2), indicating that  $\sim$ 68% of the variance in observed CO<sub>2</sub> is shared with the benthic stack. This is similar to that  
310 reported in ordinary linear least-squares regression ( $R^2=0.70$ ) by Berends *et al.* (2021b). Importantly, there is no  
311 evidence in this scatter plot for departure from the linear relationship at high or low CO<sub>2</sub> or benthic  $\delta^{18}\text{O}$  levels.

312 Second, following the approach of Chalk *et al.*, 2017 and interpreting the upper 25<sup>th</sup> percentile of CO<sub>2</sub> data as  
313 representing mean interglacial stage CO<sub>2</sub> and the lower 25<sup>th</sup> percentile of CO<sub>2</sub> data as representing mean glacial  
314 stages CO<sub>2</sub> levels, we see that our predicted interglacial mean value for the past 800 kyr ( $253.1 \pm 2.3$  ppm)  
315 closely overlaps with the observed interglacial mean value ( $253.9 \pm 4.1$  ppm) and similarly, the predicted glacial  
316 stage mean ( $199.7 \pm 1.7$  ppm) closely overlaps with the observed glacial stage mean ( $202.0 \pm 3.2$  ppm). Third,  
317 the predictions are remarkably insensitive to bootstrap analysis in which 50 % of that data are omitted with each  
318 iteration of the GLS model. Such insensitivity to the bootstrap analysis and accurate prediction of glacial *and*  
319 interglacial state CO<sub>2</sub> values would be unlikely in the case of major non-linear dependencies between the LR04  
320 predictor and CO<sub>2</sub> response variables. Fourth, non-linear approaches would risk generating an improved fit due  
321 to statistical artefacts that do not meaningfully relate to any dependence between benthic  $\delta^{18}\text{O}$  and CO<sub>2</sub>. Finally,  
322 the specific causes and sources and sinks involved in glacial to interglacial and millennial-scale CO<sub>2</sub> variations  
323 remain poorly constrained (e.g. Archer *et al.*, 2000; Sigman *et al.*, 2010; Gottschalk *et al.*, 2019). Given this  
324 process-uncertainty, the GLS model fits our criteria of the simplest reasonable model. Further, the use of benthic  
325  $\delta^{18}\text{O}$  to predict atmospheric CO<sub>2</sub> has precedence; in response to the EPICA challenge (Wolff *et al.*, 2004) N.  
326 Shackleton predicted atmospheric CO<sub>2</sub> out to 800 kyr, based on a number of benthic  $\delta^{18}\text{O}$  records from the East  
327 Pacific (Wolff, 2005).

328

329 There are several caveats with blue ice data that may affect its use to evaluate our GLS model predictions. The  
330 blue ice data may have been subject to diffusional smoothing of CO<sub>2</sub> (e.g. Yan *et al.*, 2019), which would act in  
331 the direction of elevating the (lower 25<sup>th</sup> percentile) assumed glacial concentrations above the glacial  
332 atmospheric values and reducing the (upper 25<sup>th</sup> percentile) assumed interglacial concentrations. There is also  
333 the potential for artificially elevated CO<sub>2</sub> concentrations in blue ice due in-situ respiration of CO<sub>2</sub> due to  
334 microbial activity in detrital matter. Respiration effects are screened for by measurements of  $\delta^{13}\text{C}$  of CO<sub>2</sub>,  
335 however it is difficult to demonstrate that all samples are unaffected (Yan *et al.*, 2019). These uncertainties  
336 support our argument that the GLS-model predictions are not rejected by the available observed BI-CO<sub>2</sub> data.

337

338 We consider the BI-CO<sub>2</sub> data to provide the most reliable measurements of CO<sub>2</sub> concentration, in the absence of  
339 a continuous ice core record across the MPT. However, further comparison of our CO<sub>2</sub> predictions can also be  
340 made against CO<sub>2</sub> proxy data from non-ice core archives (Fig 4A). We consider here  $\delta^{11}\text{B}$ -based atmospheric  
341 CO<sub>2</sub> reconstructions (Chalk *et al.*, 2017, Dyez *et al.* 2018 and Guillermic *et al.* 2022) and a recent atmospheric  
342 CO<sub>2</sub> reconstruction from  $\delta^{13}\text{C}$  of leaf wax (Yamamoto *et al.*, 2022). The continuous  $\delta^{11}\text{B}$ -based reconstructions  
343 of Dyez *et al.*, (2018) overlap PRED-CO<sub>2</sub> from  $\sim 1.38 - 1.5$  Mya while the Chalk *et al.*, (2017) reconstruction  
344 overlaps PRED-CO<sub>2</sub> from 1.09 – 1.43 Mya. Discrete reconstructions from Guillermic *et al.* (2022) are  
345 distributed non-uniformly across the 800 to 1.5 Mya interval. For the two continuous  $\delta^{11}\text{B}$ -based reconstructions  
346 (Chalk *et al.*, (2017) and Dyez *et al.*, (2018)) the glacial CO<sub>2</sub> levels appear consistent with the PRED-CO<sub>2</sub>  
347 record, within their reported 30 – 60 ppm uncertainties. However,  $\delta^{11}\text{B}$ -based interglacial stages in these  
348 reconstructions exceed those of the PRED-CO<sub>2</sub> record (Fig. 4A). The Guillermic *et al.* (2022) reconstructions  
349 suggest a larger range of CO<sub>2</sub> concentrations than the overlapping intervals of PRED-CO<sub>2</sub> and of the two  
350 continuous  $\delta^{11}\text{B}$ -based reconstructions (Fig. 4A). The large range of the Guillermic *et al.* (2022) data and the  
351 high interglacial maxima in the Chalk *et al.* (2017) and Dyez *et al.*, (2018) data, all significantly exceed the

352 range and interglacial maxima from the BI-CO<sub>2</sub> estimates. These discrepancies internally between different  
353  $\delta^{11}\text{B}$ -based CO<sub>2</sub> reconstructions and between the  $\delta^{11}\text{B}$ -based reconstructions and the BI-CO<sub>2</sub> data, may be due to  
354 uncertainties associated with the  $\delta^{11}\text{B}$  proxy transfer function. The  $\delta^{11}\text{B}$ -based CO<sub>2</sub> reconstructions are  
355 dependent on assumptions about multiple components of the carbonate system, including local marine carbon  
356 chemistry and the CO<sub>2</sub> saturation state in the past and (Hönisch *et al.*, 2009). Evidence that  $\delta^{11}\text{B}$ -based  
357 reconstructions may overestimate interglacial stage CO<sub>2</sub> is also seen in data from Chalk *et al.*, (2017) spanning  
358 ca. 0–250 kya, where the  $\delta^{11}\text{B}$ -based interglacial CO<sub>2</sub> levels exceed the continuous ice core CO<sub>2</sub> record by up to  
359 ca. 30 ppm.

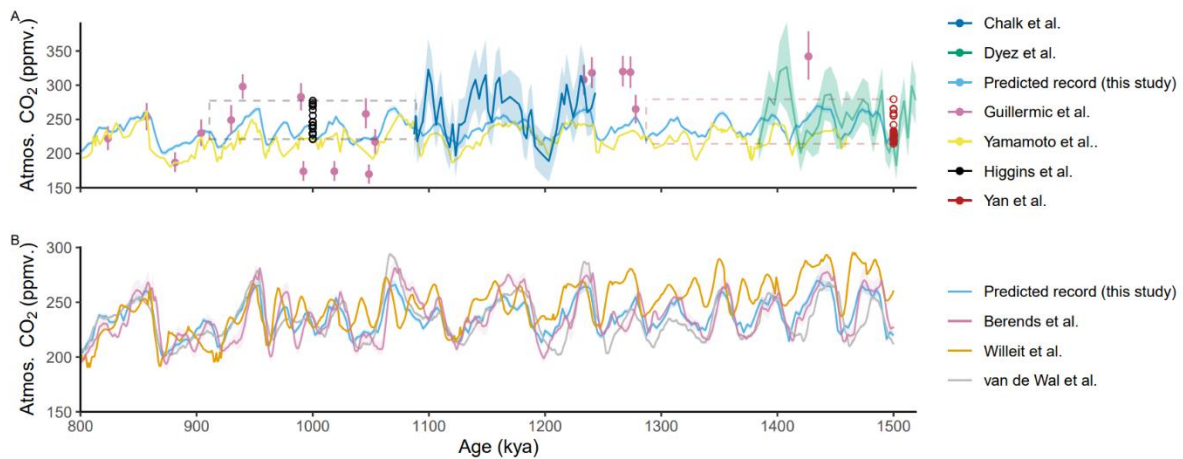
360

361 By comparison, the  $\delta^{13}\text{C}$  of leaf wax data (Yamamoto *et al.*, 2022) has a similar glacial to interglacial range as  
362 PRED-CO<sub>2</sub>, but a ca. 20ppm lower mean concentration than our predictions (Fig 4A). Hence, our PRED-CO<sub>2</sub>  
363 data fall lower than interglacial  $\delta^{11}\text{B}$ -based interglacial levels but are higher than the  $\delta^{13}\text{C}$  of leaf-wax based  
364 estimate. The strong spread between these different proxies and the large associated uncertainty of the  
365 alternative marine and leaf wax proxy-CO<sub>2</sub> reconstructions mean that we do not find cause from the existing  
366 CO<sub>2</sub> proxy data to reject our predictions nor our associated null-hypothesis.

367

368 We also compare our predictions to existing more complex model simulations (Fig 4B.). First, against a  
369 transient simulation using an intermediate-complexity earth system model (CLIMBER-2) by Willeit *et al.*  
370 (2019). This study suggests a combination of gradual regolith removal and atmospheric CO<sub>2</sub> decline can explain  
371 the long-term climate variability over the past 3 Myr. Second, against a longer-term reconstruction by van de  
372 Wal *et al.* (2011), which uses benthic  $\delta^{18}\text{O}$  that utilises deep-sea benthic isotope records to reconstruct a  
373 continuous CO<sub>2</sub> record over the past 20 Myr. Third, a CO<sub>2</sub> reconstruction based on an inverse forward-  
374 modelling approach forced by the LR04 benthic stack, in which the forward model is incrementally updated  
375 through interaction with general circulation model snapshots and the ANICE 3-D ice-sheet-shelf model  
376 (Berends *et al.* 2021b). Our simple GLS model demonstrates a similar long-term trend and timing of glacial-  
377 interglacial signals and an atmospheric CO<sub>2</sub> level that sits approximately mid-way between the van de Wal *et al.*  
378 (2011), and Willeit *et al.* (2019) models and is remarkably similar to the Berends *et al.* (2021b) reconstruction,  
379 despite their different approach. Notably the Berends *et al.* reconstruction shows greater glacial to interglacial  
380 amplitude in the CO<sub>2</sub> signal compared to our GLS-model. The decreasing linear trend in CO<sub>2</sub> in Willeit *et al.*  
381 (2019), which is not seen in the other reconstructions, was directly prescribed in that study to induce Northern  
382 Hemisphere glaciation at 2.6 Myr ago.

383



384  
 385 **Figure 4: A) Predicted CO<sub>2</sub> (this work) compared to observed, proxy CO<sub>2</sub> estimates from a range of other**  
 386 **sources:  $\delta^{11}\text{B}$ -based pCO<sub>2</sub> reconstructions and measurements by Dyez *et al.* (2018), Guillermic *et al.***  
 387 **(2022); Chalk *et al.*, (2017); blue ice CO<sub>2</sub> measurements by Yan *et al.* (2019) and Higgins *et al.* (2015);**  
 388  **$\delta^{13}\text{C}$  leaf wax proxy reconstructions by Yamamoto *et al.* (2022). The dashed boxes indicate the dating**  
 389 **uncertainty and range of the respective BI-CO<sub>2</sub> records. B) Our predicted record compared to various**  
 390 **model simulations: a regolith removal hypothesis simulation by Willeit *et al.* (2019); and inverse-model**  
 391 **based CO<sub>2</sub> reconstructions by van de Wal *et al.* (2011), and Berends *et al.*, (2021b).**

392  
 393 A complete and critical test of our and other CO<sub>2</sub> predictions awaits the upcoming analysis of the continuous  
 394 oldest ice core records. We now discuss some potential applications of the PRED-CO<sub>2</sub> record for hypothesis  
 395 testing on the cause of the MPT.

396  
 397 PRED-CO<sub>2</sub> shows a long-term decline in glacial CO<sub>2</sub> across the MPT, but no long-term decrease in interglacial  
 398 CO<sub>2</sub>. This pattern is consistent with the boron-isotope-based CO<sub>2</sub> reconstructions shown earlier, where it is often  
 399 described as an increase in the interglacial to glacial CO<sub>2</sub> difference (e.g., Chalk *et al.*, 2017; Hönlisch *et al.*,  
 400 2009). Chalk *et al.* (2017) concludes that the MPT was initiated by a change in ice sheet dynamics and that  
 401 longer and higher-ice volume post-MPT ice ages are sustained by carbon cycle feedbacks, in particular dust  
 402 fertilisation of the Southern Ocean. That fact that our LR04-based prediction of CO<sub>2</sub> captures this same trend,  
 403 with predicted glacial CO<sub>2</sub> fairly constant from 1.5 to ca. 1.0 Mya before declining from 1.0 to 0.6 kya, reflects  
 404 that LR04 benthic stack also features an increase in the interglacial to glacial benthic  $\delta^{18}\text{O}$  difference across this  
 405 same interval, which is dominated by the glacial stage changes (Fig 3A.). Here, a comparison of PRED-CO<sub>2</sub> to  
 406 a realised continuous oldest ice core record will be of value. The agreement or disagreement would inform on  
 407 the proportionality of the CO<sub>2</sub> coupling with ice volume; if there were a major new or non-linear process across  
 408 the MPT that changed the nature of coupling between CO<sub>2</sub> and ice volume the PRED-CO<sub>2</sub> and observed CO<sub>2</sub>  
 409 records would be expected to diverge.

410  
 411 Another avenue to use the PRED-CO<sub>2</sub> record for hypothesis testing on the cause of the MPT concerns the phase  
 412 locking hypothesis. The phase locking hypothesis is proposed to explain the absence of precession-related (23  
 413 kyr) periods in the LR04 benthic stack prior to the MPT (Fig 1), despite the strong precession cycle in insolation  
 414 (Raymo *et al.*, 2006, Morée *et al.*, 2021). The key concept is that prior to the MPT the Northern Hemisphere and

415 Antarctic ice sheets were responsive (in ice volume) to insolation changes in the precession band, but because  
416 precession forcing is out of phase between the hemispheres, the ice volume changes were opposing between the  
417 hemispheres and therefore cancelled in the benthic stack. This cancellation of the precession signal left  
418 insolation forcing in the 41 kyr obliquity band to dominate globally integrated ice volume changes expressed in  
419 the benthic stack. A transition from a smaller and more dynamic terrestrial-terminating Antarctic ice sheet to a  
420 larger and more stable marine-terminating ice sheet with cooling climate across the MPT (e.g. Elderfield *et al.*,  
421 2012) is then proposed to remove sensitivity of Antarctic ice volume to precession forcing and to suppress ice  
422 sheet sensitivity to the obliquity band in favour of quasi-100kyr ice volume changes that are in phase between  
423 the hemispheres (Raymo *et al.*, 2006).

424

425 Recently presented data from Yan *et al.* (2022), lend some support to the phase locking hypothesis, specifically  
426 with evidence that pre-MPT Antarctic temperature (and by extension ice volume) is positively correlated with a  
427 local precession-band insolation proxy based on the oxygen to nitrogen ratio of trapped air (Yan *et al.*, 2022).  
428 Whereas the correlation becomes negative in the blue ice and continuous ice core data in the post-MPT record.  
429 If Yan *et al.*, (2022) is correct and the phase locking hypothesis holds, then an implication is that prior to the  
430 MPT, Antarctic climate, Antarctic ice volume and by extension Southern Ocean climate conditions, would fall  
431 out of phase with the LR04 benthic stack. To now extend the argument to potential impacts on CO<sub>2</sub> exchange, if  
432 the phase locking hypothesis holds, then prior to the MPT the Antarctic and Southern Ocean climate conditions  
433 and by extension the Southern Ocean mechanisms of CO<sub>2</sub> exchange described earlier, would also be expected to  
434 fall out of phase with the benthic stack. Since our regression model assumes continuation of the in-phase  
435 relationship between the benthic stack and Antarctic and Southern Ocean climate conditions (as inherited from  
436 the post-MPT training data) we would expect to see major disagreement between our pre-MPT CO<sub>2</sub> predictions  
437 and a realised oldest ice continuous ice core CO<sub>2</sub> record.

438

## 439 **5 Summary and Conclusions**

440 In this study we have used a simple generalised least squares (GLS) model to predict atmospheric CO<sub>2</sub> from the  
441 LR04 benthic  $\delta^{18}\text{O}$  stack for the period spanning the mid-Pleistocene transition, 800–1500 kyr. Our CO<sub>2</sub>  
442 prediction is therefore based on the assumption that the physical processes linking CO<sub>2</sub>, sea level, global ice  
443 volume and ocean temperature over the past 800 kyr do not fundamentally change across the 800–1500 kya time  
444 period. The null-hypothesis is deliberately simplistic on the basis that differences between our predictions and  
445 observed or proxy CO<sub>2</sub> records may be revealing of the physical processes involved in the mid-Pleistocene  
446 Transition.

447

448 We made initial tests of the null hypothesis by comparing our predicted CO<sub>2</sub> record to existing discrete blue ice  
449 CO<sub>2</sub> records and other non-ice-core proxy-CO<sub>2</sub> records from the 800–1500 kyr interval. Our predicted CO<sub>2</sub>  
450 concentrations do not show any systematic departure from observed blue ice CO<sub>2</sub> concentrations. The  
451 predictions are marginally lower (during glacial *and* interglacial stages) than those observed in blue ice from  
452  $1000 \pm 89$  kya and marginally higher than observed in blue ice data from  $1.5 \text{ Mya} \pm 213$  kyr. Our predictions  
453 were generally lower than interglacial  $\delta^{11}\text{B}$ -based-CO<sub>2</sub> reconstructions, but higher than recent  $\delta^{13}\text{C}$  of leaf-wax  
454 based CO<sub>2</sub> reconstructions. Overall, we do not find clear evidence from the existing blue ice or proxy CO<sub>2</sub> data

455 to reject our predictions nor our associated null-hypothesis. The definitive test of our and other CO<sub>2</sub> predictions  
456 therefore awaits the future analysis of the upcoming continuous oldest ice core records. The PRED-CO<sub>2</sub> record  
457 presented here should provide a useful comparison to forthcoming oldest ice core records and opportunity to  
458 provide further constraints on the processes involved in the MPT.

459

#### 460 **Author contributions**

461 Project design by JBP, TRV and JRWM and supervision by TRV and JBP. Data analysis and figures by JRWM  
462 with input from all authors. Writing led by JRMV and JBP. All authors contributed to and agreed on the final  
463 version of the manuscript.

464

#### 465 **Competing interests**

466 The authors declare that they have no competing interests.

467

#### 468 **Disclaimer**

469 This study, to the best of the author(s) knowledge and belief, contains no material previously published or  
470 written by another person, except where due reference is made in the text of the study.

471

#### 472 **Acknowledgements**

473 We acknowledge assistance from Simon Wotherspoon (Institute for Marine and Antarctic Studies) in  
474 appropriate model selection methods. This research was supported by the Australian Government through  
475 Australian Antarctic Science projects 4632, the Million Year Ice Core (MYIC) Project and by the Australian  
476 Government Department of Industry Science Energy and Resources, grant ASCI000002.

477

#### 478 **Data availability**

479 PRED-CO<sub>2</sub> data (0 to 1.5 Myr) will be publicly archived at the Australian Antarctic Data Centre  
480 (<https://data.aad.gov.au/> >>full link provided upon publication<<).

481

#### 482 **References**

- 483 Archer, D., Winguth, A., D. Lea, and Mahowald, N.: What caused the glacial/interglacial atmospheric  
484 pCO<sub>2</sub> cycle?, *Rev. Geophys.*, 38, 159–189, 2000, <https://doi.org/10.1029/1999RG000066>, 2000.
- 485
- 486 Bazin, L., Landais, A., Lemieux-Dudon, B., Toyé Mahamadou Kele, H., Veres, D., Parrenin, F., Martinerie, P.,  
487 Ritz, C., Capron, E., Lipenkov, V., Loutre, M.-F., Raynaud, D., Vinther, B., Svensson, A., Rasmussen, S.,  
488 Severi, M., Blunier, T., Leuenberger, M., Fischer, H., Masson-Delmotte, V., Chappellaz, J., and Wolff, E.: An  
489 optimized multi-proxies, multi-site Antarctic ice and gas orbital chronology (AICC2012): 120-800 ka, *Clim.*  
490 *Past*, 9, 1715-1731, <https://doi.org/10.5194/cp-9-1715-2013>, 2013.
- 491
- 492 Bereiter, B., Eggleston, S., Schmitt, J., Nehrbass-Ahles, C., Stocker, T. F., Fischer, H., Kipfstuhl, S., and  
493 Chappellaz, J.: Revision of the EPICA Dome C CO<sub>2</sub> record from 800 to 600 ky before present, *Geophys. Res.*  
494 *Let.*, 42, 542-549, <https://doi.org/10.1002/2014gl061957>, 2015.
- 495
- 496 Berends, C. J., Köhler, P., Lourens, L. J., and van de Wal, R. S. W.: On the cause of the mid-Pleistocene  
497 transition., *Rev. Geophys.*, 59, e2020RG000727. <https://doi.org/10.1029/2020RG000727>, 2021a.
- 498
- 499 Berends, C. J., de Boer, B., and van de Wal, R. S. W.: Reconstructing the evolution of ice sheets, sea level, and  
500 atmospheric CO<sub>2</sub> during the past 3.6 million years. *Clim. Past*, 17, 361–377, [http://doi.org/10.5194/cp-17-361-](http://doi.org/10.5194/cp-17-361-2021)  
501 2021, 2021b.

502  
503 Berger, A., Li, X. S., and Loutre, M. F.: Modelling northern hemisphere ice volume over the last 3Ma,  
504 Quaternary. Sci. Rev., 18, 1-11, [https://doi.org/10.1016/S0277-3791\(98\)00033-X](https://doi.org/10.1016/S0277-3791(98)00033-X), 1999.  
505  
506 Broecker, W.S.: Glacial to interglacial changes in ocean chemistry, Prog. Oceanogr., 11 (2), 151-197.  
507 [https://doi.org/10.1016/0079-6611\(82\)90007-6](https://doi.org/10.1016/0079-6611(82)90007-6), 1982.  
508  
509 Chalk, T., Hain, M., Foster, G., Rohling, E., Sexton, P., Badger, M., Cherry, S., Hasenfratz, A., Haug, G.,  
510 Jaccard, S., Martínez-García, A., Pälike, H., Pancost, R., and Wilson, P.: Causes of ice age intensification across  
511 the Mid-Pleistocene Transition, P. Natl. Acad. Sci. USA., 114, 13114-13119,  
512 <https://doi.org/10.1073/pnas.1702143114>, 2017.  
513  
514 Clark, P. U., Archer, D., Pollard, D., Blum, J. D., Rial, J. A., Brovkin, V., Mix, A. C., Pisias, N. G., and Roy,  
515 M.: The middle Pleistocene transition: characteristics, mechanisms, and implications for long-term changes in  
516 atmospheric pCO<sub>2</sub>, Quat. Sci. Rev., 25, 3150-3184, <https://doi.org/10.1016/j.quascirev.2006.07.008>, 2006.  
517  
518 Clark, P. U. and Pollard, D.: Origin of the Middle Pleistocene Transition by ice sheet erosion of regolith,  
519 Paleooceanography, 13, 1-9, <https://doi.org/10.1029/97pa02660>, 1998.  
520  
521 Dyez, K.A., Hönisch, B., and Schmidt, G.A.: Early Pleistocene obliquity-scale pCO<sub>2</sub> variability at ~1.5 million  
522 years ago. Paleooceanogr. Paleoclimatol., 33, no. 11, 1270-1291, <https://doi.org/10.1029/2018PA003349>, 2018.  
523  
524 Elderfield, H., Ferretti, P., Greaves, S., Crowhurst, S., McCave, N., and Piotrowski, A.M.: Evolution of Ocean  
525 Temperature and Ice Volume Through the Mid-Pleistocene Climate Transition, Science, 337,704-709,  
526 <https://doi.org/10.1126/science.1221294>, 2012.  
527  
528 Gottschalk, J., Battaglia, G., Fischer, H., Frölicher, T.L., Jaccard, S.L., Jeltsch-Thömmes, A., Joos, F., Köhler,  
529 P., Meissner, K.J., Menviel, L., Nehrbass-Ahles, C., Schmitt, J., Schmittner, A., Skinner, L.C., and Stocker,  
530 T.G.: Mechanisms of millennial-scale atmospheric CO<sub>2</sub> change in numerical model simulations, Quaternary.  
531 Sci. Rev., 220, 30-74, <https://doi.org/10.1016/j.quascirev.2019.05.013>, 2019.  
532  
533 Guillermic, M., Misra, S., Eagle, R., and Tripathi, A.: Atmospheric CO<sub>2</sub> estimates for the Miocene to Pleistocene  
534 based on foraminiferal δ<sup>11</sup>B at Ocean Drilling Program Sites 806 and 807 in the Western Equatorial Pacific,  
535 Clim. Past, 18(2), 183-207, <https://doi.org/10.5194/cp-18-183-2022>, 2022.  
536  
537 Hasenfratz, A. P., Jaccard, S. L., Martínez-García, A., Sigman, D. M., Hodell, D. A., Vance, D., Bernasconi, S.  
538 M., Kleiven, H. F., Haumann, F. A., and Haug, G. H.: The residence time of Southern Ocean surface waters and  
539 the 100,000-year ice age cycle, Science, 363, 1080, <https://doi.org/10.1126/science.aat7067>, 2019.  
540  
541 Higgins, J. A., Kurbatov, A. V., Spaulding, N. E., Brook, E., Introne, D. S., Chimiak, L. M., Yan, Y.,  
542 Mayewski, P. A., and Bender, M. L.: Atmospheric composition 1 million years ago from blue ice in the Allan  
543 Hills, Antarctica, P. Natl. Acad. Sci. USA., 112, 6887, <https://doi.org/10.1073/pnas.1420232112>, 2015.  
544  
545 Hönisch, B., Hemming, N. G., Archer, D., Siddall, M., and McManus, J. F.: Atmospheric Carbon Dioxide  
546 Concentration Across the Mid-Pleistocene Transition, Science, 324, 1551,  
547 <https://doi.org/10.1126/science.1171477>, 2009.  
548  
549 Huybers, P., & Wunsch, C. (2005). Obliquity pacing of the late Pleistocene glacial terminations. *Nature*,  
550 434(7032), 491-494.  
551  
552 International Panel on Climate Change: Climate change 2001; IPCC third assessment report, IPCC, Geneva,  
553 2001.  
554  
555 International Partnerships in Ice Core Sciences: The oldest ice core: A 1.5 million year record of climate and  
556 greenhouse gases from Antarctica [White paper]. [https://igbp-](https://igbp-scor.pages.unibe.ch/sites/default/files/download/docs/working_groups/ipics/white-papers/ipics_oldaa_final.pdf)  
557 [scor.pages.unibe.ch/sites/default/files/download/docs/working\\_groups/ipics/white-papers/ipics\\_oldaa\\_final.pdf](https://igbp-scor.pages.unibe.ch/sites/default/files/download/docs/working_groups/ipics/white-papers/ipics_oldaa_final.pdf),  
558 accessed 06/12/2023, 2020.  
559  
560 Jouzel, J., Masson-Delmotte, V., Cattani, O., Dreyfus, G., Falourd, S., Hoffmann, G., Minster, B., Nouet, J.,  
561 Barnola, J. M., Chappellaz, J., Fischer, H., Gallet, J. C., Johnsen, S., Leuenberger, M., Loulergue, L., Luethi, D.,

562 Oerter, H., Parrenin, F., Raisbeck, G., Raynaud, D., Schilt, A., Schwander, J., Selmo, E., Souchez, R., Spahni,  
563 R., Stauffer, B., Steffensen, J. P., Stenni, B., Stocker, T. F., Tison, J. L., Werner, M., and Wolff, E. W.: Orbital  
564 and Millennial Antarctic Climate Variability over the Past 800,000 Years, *Science*, 317, 793,  
565 <https://doi.org/10.1126/science.1141038>, 2007.

566  
567 Lisiecki, L. E. and Raymo, M. E.: A Pliocene-Pleistocene stack of 57 globally distributed benthic  $\delta^{18}\text{O}$  records,  
568 *Paleoceanography*, 20, PA1003, <https://doi.org/10.1029/2004pa001071>, 2005.

569  
570 Martínez-García, A., Sigman, D.M., Ren, H., Anderson, R.F., Straub, M., Hodell, D.A., Jaccard, S.L., Eglinton,  
571 T.I., and Haug, G.H.: Iron fertilization of the subantarctic ocean during the last ice age, *Science*, 343 (6177),  
572 1347-1350, <https://doi.org/10.1126/science.1246848>, 2014.

573  
574 McClymont, E.L., Sostdian, S.M., and Rosell-Melé, A.: Pleistocene sea-surface temperature evolution: Early  
575 cooling, delayed glacial intensification, and implications for the mid-Pleistocene transition. *Earth. Sci. Rev.*,  
576 123, 173-193, <https://doi.org/10.1016/j.earscirev.2013.04.006>, 2013.

577  
578 Millero, F. J.: Thermodynamics of the carbon dioxide system in the oceans, *Geochim. Cosmochim. Acta.*, 59,  
579 661-677, [https://doi.org/10.1016/0016-7037\(94\)00354-O](https://doi.org/10.1016/0016-7037(94)00354-O), 1995.

580  
581 Morée, A. L., Sun, T., Bretones, A., Straume, E. O., Nisancioglu, K., and Gebbie, G.: Cancellation of the  
582 precessional cycle in  $\delta^{18}\text{O}$  records during the Early Pleistocene. *Geophys. Res. Lett.*, 48,  
583 e2020GL090035. <https://doi.org/10.1029/2020GL090035>, 2021.

584  
585 Petit, J. R., Jouzel, J., Raynaud, D., Barkov, N. I., Barnola, J. M., Basile, I., Bender, M., Chappellaz, J., Davis,  
586 M., Delaygue, G., Delmotte, M., Kotlyakov, V. M., Legrand, M., Lipenkov, V. Y., Lorius, C., Pépin, L., Ritz,  
587 C., Saltzman, E., and Stievenard, M.: Climate and atmospheric history of the past 420,000 years from the  
588 Vostok ice core, Antarctica, *Nature*, 399, 429-436, <https://doi.org/10.1038/20859>, 1999.

589  
590 Raymo, M., Lisiecki, L., and Nisancioglu, K.: Plio-Pleistocene Ice Volume, Antarctic Climate, and the Global  
591  $18\text{O}$  Record, *Science*, 313, 492-495, <https://doi.org/10.1126/science.1123296>, 2006.

592  
593 Raymo, M., Ruddiman, W., and Froelich, P.: Influence of Late Cenozoic mountain building on ocean  
594 geochemical cycles, *Geology*, 16, 649-653, [https://doi.org/10.1130/0091-](https://doi.org/10.1130/0091-7613(1988)016<0649:IOLCMB>2.3.CO;2)  
595 [7613\(1988\)016<0649:IOLCMB>2.3.CO;2](https://doi.org/10.1130/0091-7613(1988)016<0649:IOLCMB>2.3.CO;2), 1988.

596  
597 Raymo, M. E.: The timing of major climate terminations, *Paleoceanography*, 12, 577-585,  
598 <https://doi.org/10.1029/97PA01169>, 1997.

599  
600 Raymo, M. E. and Huybers, P.: Unlocking the mysteries of the ice ages, *Nature*, 451, 284-285,  
601 <https://doi.org/10.1038/nature06589>, 2008.

602  
603 Röthlisberger, R., Bigler, M., Wolff, E. W., Joos, F., Monnin, E., and Hutterli, M. A.: Ice core evidence for the  
604 extent of past atmospheric  $\text{CO}_2$  change due to iron fertilisation, *Geophys. Res. Lett.*, 31, L16207,  
605 <https://doi.org/10.1029/2004GL020338>, 2004.

606  
607 Ruddiman, W. F., Raymo, M. E., Martinson, D. G., Clement, B. M., and Backman, J.: Pleistocene evolution:  
608 Northern hemisphere ice sheets and North Atlantic Ocean, *Paleoceanography*, 4, 353-412,  
609 <https://doi.org/10.1029/PA004i004p00353>, 1989.

610  
611 Shackleton, N. J. and Pisias, N. G.: Atmospheric Carbon Dioxide, Orbital Forcing, and Climate. In: *The Carbon*  
612 *Cycle and Atmospheric  $\text{CO}_2$ : Natural Variations Archean to Present*, <https://doi.org/10.1029/GM032p0303>,  
613 1985.

614  
615 Shugi, H., The older the ice, the better the science. *Adv. Polar Sci.*, 23, 121-122,  
616 <https://doi.org/10.13679/j.advps.2022.0004>, 2022.

617  
618 Stephens, B.B., Keeling, R.F.: The influence of Antarctic sea ice on glacial–interglacial  $\text{CO}_2$  variations. *Nature*,  
619 404, 171–174, <https://doi.org/10.1038/35004556>, 2000.

620



621 Tzedakis, P. C., Crucifix, M., Mitsui, T., and Wolff, E. W.: A simple rule to determine which insolation cycles  
622 lead to interglacials, *Nature*, 542, 427-432, <https://doi.org/10.1038/nature21364>, 2017.  
623

624 Ushie, H., and Matsumoto, K.: The role of shelf nutrients on glacial-interglacial CO<sub>2</sub>: A negative  
625 feedback, *Global Biogeochem. Cy.*, 26, GB2039, <https://doi.org/10.1029/2011GB004147>., 2012.  
626

627 van de Wal, R. S. W., de Boer, B., Lourens, L. J., Köhler, P., and Bintanja, R.: Reconstruction of a continuous  
628 high-resolution CO<sub>2</sub> record over the past 20 million years. *Clim. Past*, 7, 1459–1469. [https://doi.org/10.5194/cp-](https://doi.org/10.5194/cp-7-1459-2011)  
629 [7-1459-2011](https://doi.org/10.5194/cp-7-1459-2011), 2011.  
630

631 Veres, D., Bazin, L., Landais, A., Toyé Mahamadou Kele.H., Lemieux-Dudon, B., Parrenin, F., Martinerie, P.,  
632 Blayo, E., Blunier, T., Capron, E., Chappellaz, J., Rasmussen, S., Severi, M., Svensson, A., Vinther, B., and  
633 Wolff, E.: The Antarctic ice core chronology (AICC2012): an optimized multi-parameter and multi-site dating  
634 approach for the last 120 thousand years, *Clim. Past*, 9, 1733-1748, <https://doi.org/10.5194/cp-9-1733-2013>,  
635 2013.  
636

637 Willeit, M., Ganopolski, A., Calov, R., and Brovkin, V.: Mid-Pleistocene transition in glacial cycles explained by  
638 declining CO<sub>2</sub> and regolith removal, *Sci. Adv.*, 5, eaav7337, doi: 10.1126/sciadv.aav7337, 2019.  
639

640 Wolff, E. W., Chappella, J., Fischer, H., Kull, C., Miller, H., Stocker, T. F., and Watson, A. J.: The EPICA  
641 challenge to the Earth system modeling community, *EOS*, 85, 363363, <https://doi.org/10.1029/2004EO380003>,  
642 2004.  
643

644 Wolff, E. W., Kull, C., Chappellaz, J., Fischer, H., Miller, H., Stocker, T. F., Watson, A. J., Flower, B., Joos, F.,  
645 Köhler, P., Matsumoto, K., Monnin, E., Mudelsee, M., Paillard, D., and Shackleton, N.: Modeling past  
646 atmospheric CO<sub>2</sub>: results of a challenge, *EOS*, 86 (38), 341-345, <http://doi.org/10.1029/2005EO380003>, 2005.  
647

648 Yamamoto, M., Clemens, S.C., Seki, O., Tsuchiya, Y., Huang, Y., O'ishi, R., and Abe-Ouchi, A.: Increased  
649 interglacial atmospheric CO<sub>2</sub> levels followed the mid-Pleistocene Transition, *Nat. Geosci.*, 15(4), 307–313,  
650 <https://doi.org/10.1038/s41561-022-00918-1>, 2022.  
651

652 Yan, Y., Bender M.I., Brook, E.J., Clifford, H.M., Kemeny, P.C., Kurbatov, A.V., Mackay, S., Mayewski,  
653 P.A., Ng, J., Severinghaus J.P., and Higgins, J.A.: Two-million-year-old snapshots of atmospheric gases from  
654 Antarctic ice, *Nature*, 574(7780), 663–666, <https://doi.org/10.1038/s41586-019-1692-3>, 2019.  
655

656 Yan, Y., Kurbatov, A.V., Mayewski, P.A., Shackleton, S., and Higgins, J.A.: Early Pleistocene East Antarctic  
657 temperature in phase with local insolation. *Nat. Geosci.*, 16, 50-55, [https://doi.org/10.1038/s41561-022-01095-](https://doi.org/10.1038/s41561-022-01095-x)  
658 [x](https://doi.org/10.1038/s41561-022-01095-x), 2022.